Nuclear Materials and Energy 19 (2019) 250–254

Contents lists available at ScienceDirect

Nuclear Materials and Energy

journal homepage: www.elsevier.com/locate/nme

Design and calibration of a retarding field energy analyzer for the LTX-β scrape off layer and modeling of electrostatic potential in a collisionless SOL

X. Zhang*[,a], D.B. Elliott[b], A. Maan[c], D.P. Boyle[a], R. Kaita[c], R. Majeski[a]

[a] Princeton Plasma Physics Laboratory, 100 Stellerator Rd, Princeton, NJ 08536, USA
[b] Oak Ridge National Laboratory, Oak Ridge, TN 37831, USA
[c] University of Tennessee Knoxville, Knoxville, TN 37996, USA

ARTICLE INFO

Keywords:
Lithium PFC
Scrape off layer
Ambipolar potential
Retarding field energy analyzer

ABSTRACT

The Lithium Tokamak eXperiment (LTX) is a spherical tokamak device designed to study lithium plasma facing components (PFCs). The lithium coated wall of LTX has been demonstrated to produce a plasma edge with high electron temperature (200 eV or greater). Plasma density in the outer scrape-off layer (SOL) is also found to be very low, around $2 \times 10^{17} m^{-3}$, as a result of the low recycling lithium boundary. The high temperature, low collisionality region of the plasma extends into the SOL. The recent upgrade to LTX-β includes installation of a neutral beam, which will provide further heating and fueling of the core plasma. Core and edge diagnostics will also be expanded. As part of this expansion, a Retarding Field Energy Analyzer (RFEA) has been developed for the SOL of LTX-β. Measurements of the ion temperature, ion energy distribution, and the local space potential will be performed in the SOL plasma using this RFEA. Upgraded high field side (HFS) and low field side (LFS) Langmuir probes will replace existing triple probes so that higher electron temperatures can be more reliably measured. The HFS probes are also positioned to give radial and vertical gradient measurements. The design of the RFEA will be presented, along with calibration data.

Since a high temperature, low collisional edge is expected for LTX-β, with a high mirror ratio near the LCFS (around 4), the majority of particles in the SOL will be mirror-trapped. Trapped particle effects will therefore become significant in the physics of the SOL plasma, and warrant further theoretical investigations. Here we present a theoretical study of the ambipolar potential formed in the collisionless SOL via differential loss of the electrons and ions, known as the Pastukhov potential in the literature. Numerical results will also be presented.

1. Introduction

Tokamak plasmas typically exhibit a peaked temperature profile as a result of the plasma cooling by high recycling walls. This temperature gradient has been known to drive instabilities and degrade plasma performance [1]. It has been predicted theoretically that a low recycling plasma facing surface in fusion devices will drastically modify the temperature profile and improve plasma performance [1,2]. One way to produce such a low recycling plasma boundary is with lithium coated plasma facing components (PFCs). The lithium PFCs are expected to retain low energy hydrogen isotopes, and to suppress neutral pressure in the edge region as a result. The edge plasma can therefore enter a high temperature, low density regime, allowing for a flat or nearly flat temperature profile across the core and scrape off layer (SOL) plasma.

The Lithium Tokamak eXperiment (LTX) is a low aspect ratio spherical tokamak (ST) designed to investigate the effects of low recycling lithium PFCs on plasma confinement and equilibria. Previously, LTX successfully demonstrated this flat temperature profile [3,4]. From Thomson Scattering measurements, the electron temperature was seen to flatten across the plasma after gas puffing was terminated, reaching around 200 eV at the last closed flux surface (LCFS). Plasma density and pressure remained peaked, with very low values of $2 \times 10^{17} m^{-3}$ and $\sim 10^{-6}$ Torr, respectively, at the LCFS. Direct measurements of space potential, ion parameters, and other SOL characteristics were not available. Nonetheless, the ion temperature was inferred from equilibrium reconstruction to fall in the range of 40–70 eV, with a similar flat profile across the core plasma [3,4]. The expansion of the SOL diagnostic set is a major part of the upgrade to LTX-β, along with the installation of a neutral beam injection (NBI) system [5].

From the aforementioned experimental observations, the LTX SOL was inferred to be highly collisionless, with the collisionality ν^*

* Corresponding author.
E-mail address: xzhang@pppl.gov (X. Zhang).

https://doi.org/10.1016/j.nme.2019.02.027
Received 28 July 2018; Accepted 19 February 2019

computed to be below 0.1 for both electrons and ions at the LCFS when the temperature profile was flat. This is a stark deviation from the conventional cold, collisional, fluid-like SOL plasmas seen in most tokamak experiments. Instead, with negligible charge exchange losses, the majority of the low field side (LFS) SOL particles are mirror trapped due to the low aspect ratio. The plasma loss rate along field lines is no longer determined by simple bulk flow at the sound speed, with characteristic time $\tau \sim 60$ μs, but by ions pitch angle scattering from trapped to passing orbits, with a much longer characteristic time $\tau_{ii} \sim 2$ ms [4].

Consequently, the traditional Debye sheath model for plasma space potential no longer holds, since it relies on a fluid description of plasma. Rather, the ambipolar potential in a collisionless SOL falls closer within the realm of magnetic mirrors, where the ambipolar potential balances the differential loss from pitch angle scattering of ions and electrons. The additional NBI system on LTX-β will fuel the plasma without cooling the edge, and is expected to increase the time that the temperature profile is flat. The SOL of LTX-β is then expected to remain in this collisionless regime for a larger fraction of the shot duration, which may have serious consequences on the transport and confinement properties of the core plasma. The formation and the properties of the ambipolar potential in a collisionless, mirror-trapped SOL therefore warrant further theoretical investigation.

In this work, we present a numerical study of the ambipolar potential in the LTX SOL, followed by the design and calibration of a Retarding Field Energy Analyzer (RFEA) to be installed onto LTX-β. This RFEA will be used to experimentally characterize the ion energy profile and the plasma potential in the SOL, and to validate the theoretical predictions.

2. Ambipolar potential in the LTX SOL

It has been well known since the early days of magnetic mirrors that a mirror-trapped plasma will develop a positive potential to balance the electron and ion loss rates [6]. This arises from the difference in pitch angle scattering times of electrons and ions at similar temperatures. To maintain ambipolarity, the bulk plasma develops a positive potential to enhance electron confinement. This potential modifies the shape of the loss cone into a hyperbola:

$$(R-1)v_{\perp}^2 = v_{\parallel}^2 + \frac{2Zq_{\alpha}\phi}{m_{\alpha}} \tag{1}$$

where $R \equiv B_{\max}/B_{\min}$ is the mirror ratio, ϕ is the electrostatic potential, and α denotes particle species. As a result, low energy electrons are trapped electrostatically while low energy ions are repelled (Fig. 1). The combined loss rates of the ions and electrons are therefore balanced, and the plasma reaches steady state.

In 1974, V. P. Pastukhov analytically derived the rate for the collisional end loss of electrons in a *square well* magnetic mirror in the presence of a positive potential [7]. The following assumptions are made in his treatment: a) both the mirror ratio and the positive potential are sufficiently large ($R \equiv B_{\max}/B_0 \gg 1$; $e\phi/T_e \gg 1$, where $B_{\max}$ is the field at the mirror throat and B_0 is the field at midplane); and b) the characteristic bounce time is significantly smaller than that of pitch angle scattering [7]. These assumptions ensure that the electron distribution function does not deviate significantly from Maxwellian, and that particles are well trapped adiabatically such that pitch angle scattering is the dominant loss mechanism.

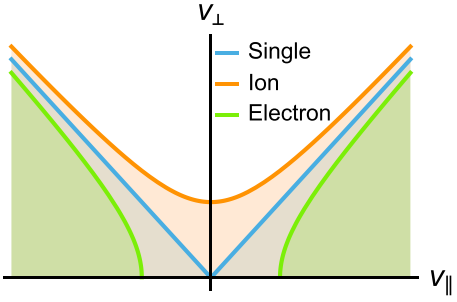

Fig. 1. Single particle loss boundary compared with the electron and the ion loss boundaries when modified by a positive potential. Loss regions are shaded. Ion-electron mass ratio is set to unity for illustrative purposes.

In the LTX SOL, because of the low collisionality produced by low-recycling PFCs and the high mirror ratio inherent to the ST geometry, the main loss mechanism is pitch angle scattering from trapped to passing orbits. We therefore expect the plasma ambipolar potential to be approximately Pastukhov.

2.1. The Pastukhov potential

To derive an expression for the Pastukhov potential, we start from the electron loss rate given in Pastukhov's 1974 analysis, corrected and generalized by Chernin et al. and Cohen et al. [7–9]:

$$\frac{dn}{dt} = -\frac{4}{\sqrt{\pi}}\frac{n}{\tau_e}\frac{1}{x}\frac{\exp(-x)}{G(R)}\int_0^{\infty} d\xi\,[e^{-\xi}\sqrt{1+\xi/x}] \tag{2}$$

where τ_e is the electron collision time, $x \equiv e\phi/T_e$ is the potential normalized with the electron temperature, and:

$$G(R) \equiv \frac{2RZ+1}{2RZ}\ln(4RZ+2). \tag{3}$$

Recall that these equations are only valid assuming a large mirror ratio and a high potential. From this point on we assume singly charged ions ($Z = 1$), since both LTX and LTX-β use hydrogen gas exclusively. The electron confinement time is then calculated from the Pastukhov loss rate:

$$\begin{aligned}\tau_{ce} &= -\frac{n}{dn/dt} \\ &= \frac{\sqrt{\pi}}{2\tau_e}x\exp(x)\frac{G(R)}{\int_0^{\infty} d\xi\,[e^{-\xi}\sqrt{1+\xi/x}]}.\end{aligned} \tag{4}$$

Because $m_i \gg m_e$, ions are approximately unaffected by the electrostatic potential compared to the electrons, per Eq. (1). The ion confinement time can then be shown from Fokker–Planck analysis to be [6]:

$$\tau_{ci} \approxeq \tau_i \log(R) \tag{5}$$

where τ_i is the ion collision time, related to τ_e as [10]

$$\tau_i = \frac{1}{\sqrt{2}}\sqrt{\frac{m_i}{m_e}}\left(\frac{T_i}{T_e}\right)^{\frac{3}{2}}\tau_e. \tag{6}$$

These confinement times are in general different, so the ambipolar potential evolves to balance them. Therefore, by setting $\tau_{ci} = \tau_{ce}$ for a given mass ratio, temperature ratio, and mirror ratio, the normalized potential x can be found from:

$$f(x) = \sqrt{\frac{2}{\pi}}\sqrt{\frac{m_i}{m_e}}\left(\frac{T_i}{T_e}\right)^{\frac{3}{2}}\frac{\log R}{G(R)} \tag{7}$$

where $f(x)$ is defined as

$$f(x) \equiv xe^x\Big/\left[\frac{\sqrt{\pi}e^x erfc(\sqrt{x})}{2\sqrt{x}}+1\right]. \tag{8}$$

Eq. (7) is transcendental, and is best solved numerically.

2.2. Numerical modeling of the LTX SOL

We aim to apply Pastukhov's square-well result to the LTX SOL to gain a qualitative understanding of its ambipolar potential. Several simplifying assumptions are made.

First, the curvature of the field lines are neglected. Assuming well-conserved magnetic moments, particles follow the field lines exactly, reducing the bounce motion to one dimension.

Second, particles are assumed to have the same initial temperature when scattered into the SOL from the LCFS, irrespective of their initial position. This is consistent with the observed flat temperature profile on LTX. The result is a different starting magnetic moment μ_0, on average, for particles loaded, or initialized, into locations with different field strengths, with larger average μ_0 corresponding to a smaller initial field strength. The mirror force seen by these particles are therefore different, with those loaded closest to the LFS midplane experiencing the strongest magnetic trap. Equivalently, these differences in the mirror force can be described as a difference in the "effective mirror ratio" that defines the loss boundary of particles loaded into that particular location.

Finally, each particle is assumed to collide only with other particles loaded at the same location. This guarantees that all scattering occurs between particles in the same magnetic trap. The ambipolar potential is then approximated to be formed by only the particles loaded into that location. In addition, this potential serves only to modify the local loss cone, and does not influence the dynamics of particles loaded elsewhere. Under these assumptions, the loss processes at any given location in the SOL can now be well approximated with a "square-well" magnetic trap. Eq. (7) can then be used to determine the ambipolar potential in the LTX SOL, using the local plasma parameters and magnetic configuration.

The magnetic geometry is taken from an MHD equilibrium reconstruction of a past LTX experiment [11]. The equilibrium is axisymmetric, and defined on a 260 by 260 grid in the $r-z$ plane that spans the entire plasma cross section. All three dimensions of the magnetic field in cylindrical coordinates (B_r, B_z, B_ϕ), the magnetic flux, and the pressure are provided on each grid point. The MHD equilibrium reconstruction assumes zero pressure in the SOL, which is not accurate, but allows the domain of interest to be easily identified: the ambipolar potential is only computed on grid points with $P = 0$.

To calculate the mirror ratio on each grid point, we need to find the maximum of the magnetic field along the field line containing that point. On LTX, since the plasma is limited on the HFS, this maximum occurs where the field line intersects the HFS limiter. Let $z_\ell(r)$ parametrize the limiter. For each coordinate (r_0, z_0) with magnetic flux $\psi(r_0, z_0) \equiv \psi_0$ in the computational domain, we find along the limiter the location $(r, z_\ell(r))$ where

$$\psi(r, z_\ell(r)) = \psi_0. \tag{9}$$

This is performed via a 1-D bisection method, with roots bracketed by the minor radius a as $r \in [R_0 - a, R_0 + a]$, where R_0 is the major radius. Therefore, the effective mirror ratio is simply $R_e(r_0, z_0) = B(r', z_\ell(r'))/B(r_0, z_0)$, where r' is the solution to Eq. (9). The obtained profile of the mirror ratio in the LTX SOL is shown in Fig. 2.

With R_e computed throughout the SOL, Eq. (7) can be numerically solved for a given temperature ratio T_i/T_e and mass ratio m_i/m_e. Fig. 2 shows the calculated Pastukhov potential in the LTX SOL for a hydrogen plasma at two different temperature ratios: $T_i/T_e = 0.2$, which is the typical value for LTX, and $T_i/T_e = 1$, which is expected on LTX-β with NBI heating.

For both temperature ratios, the ambipolar potential in the SOL falls significantly below the usual Debye sheath potential, whose value is typically around $e\phi_D/T_e \sim 3$–5 for hydrogen plasma. For an electron temperature of 200 eV, for example, the Debye sheath potential is around $5T_e \sim 1$ keV, while the Pastukhov potential is around $0.5T_e \sim 100$ eV, which is an order of magnitude reduction. This means that passing ions will gain a substantially smaller amount of energy during their transit into the limiter when the SOL is collisionless. Combined with the mirror trapping of the bulk ion population, both heat and particle flux will be dramatically lower than that expected from conventional sheath calculations with a high edge temperature. Consequently, the sputtering yield will be substantially reduced as well.

Lastly, the potential gradient in the SOL is no longer confined to a narrow region in front of the limiting surfaces. Instead, the potential varies across the entire SOL, in both radial and parallel directions. The resultant parallel electric field should contribute to the ejection of low energy sputtered ions from the lithium coated PFCs, and should protect the core plasma from contamination [4].

3. Retarding field energy analyzer for LTX-β ion diagnostics

As part of the upgrade to LTX-β, several new diagnostics are being implemented to provide direct measurements of the SOL plasma parameters, including Langmuir probes on both the LFS and the HFS, edge fluctuation probes, and a Retarding Field Energy Analyzer (RFEA). In addition to providing basic characterizations of the SOL plasma, observations from these new diagnostics will serve to verify the numerical predictions made in the previous section. Here we focus on the design and testing of the RFEA.

An RFEA has been purchased and adapted from Kimball Physics (model FC-71) to characterize the ion energy and space potential of the SOL plasma in LTX-β (Fig. 3). The analyzer consists of a set of grids that can each be electrically biased, and a Faraday cup (FC) behind the grids to collect particle current. The grids can be biased to measure either ion or electron temperature (T_i or T_e mode).

In T_i mode, the potential on the grids is such that: a) the front grid (G) facing the bulk plasma is biased sufficiently negative relative to plasma potential, to reflect incident electrons, b) the intermediate "retarding" grid (R) is biased positive relative to the FC, with a potential that can be varied to selectively transmit only those ions with energies higher than the bias voltage, and c) the final grid (S) is biased negative relative to the FC, to suppress secondary electrons emitted from ion impact on the collecting surface [12,13]. A diagram for this potential setup is shown in Fig. 3. In T_e mode, the potential setup is similar, but with the third grid variably biased instead of the second, to selectively collect high energy electrons [12]. Note that the RFEA can also be used as a standing Faraday Cup when the positive sweep is not applied in T_i mode.

Because one of the key features of an RFEA is to transmit only a single species, space charge naturally builds up between the grids. It is well known that excess space charge between electrodes distorts the potential within the bounded volume and limits the current. In an RFEA, the region between the front electron repeller grid and the intermediate ion retarding grid (region II, Fig. 3b) is the most likely to experience space charge limitation [12–15]. This effect is particularly important when the retarding grid bias is lower than the average energy of the collected ions, which is the case when the bias is near or below the plasma potential. Therefore, space charge limitation directly degrades the accuracy of plasma potential measurements, and may also distort temperature measurements [15].

The threshold of this space charge limitation can be found according to the Child-Langmuir law. It can be shown that the limitation is avoided if the grid spacing d and the Debye length λ_d of the plasma in front of the RFEA satisfy $d < 4\lambda_d$ [13]. For typical LTX plasma parameters in the edge ($n_e \sim 10^{17}\mathrm{m}^{-3}$, $T_e \approx 200$ eV, and $T_i \approx 40$ eV), $\lambda_d \sim 0.4$ mm. Since the grid spacing in the RFEA is fairly large at 2 mm, the Debye length is marginally too low to avoid space charge saturation.

Therefore, a set of tungsten masks have been developed to increase the Debye length of the plasma in front of the analyzer by reducing the incident particle flux (Fig. 3c, inset). The masks are fabricated with 20 μm thick tungsten foil, with an array of ~ 300 holes of various diameters laser drilled within a 5 mm wide radial aperture, reducing particle flux into the analyzer by 2 orders of magnitude. The foils are spot-welded onto 0.020 in. thick, 1 in. × 1 in. square TZM plates, with screw holes that align with those on the RFEA. When mounted in front of the RFEA, it serves the dual purpose of reducing particle flux into the

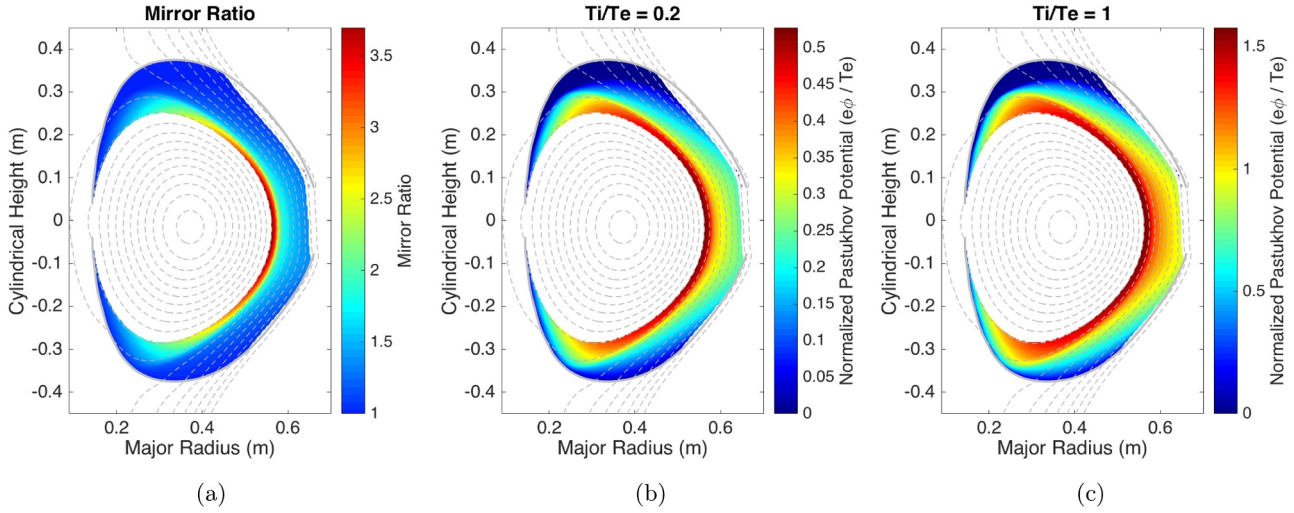

Fig. 2. (a) Effective mirror ratio in the LTX SOL. (b) Calculated ambipolar potential at $T_i/T_e = 0.2$, which corresponds to typical LTX parameters where $T_i \sim$ 40eV and $T_e \sim$ 200eV. (c) Calculated ambipolar potential at $T_i/T_e = 1$, which is projected for LTX-β.

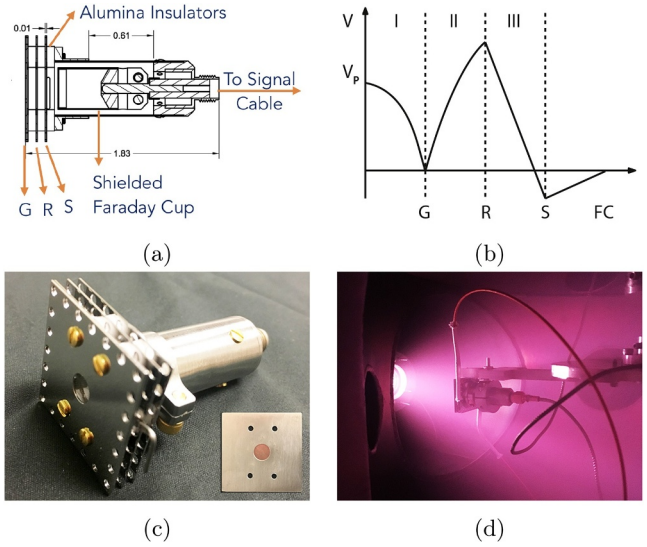

Fig. 3. (a) The RFEA cross section. (b) Grid potential setup to measure ion temperature and plasma potential. (c) The RFEA. (inset) Tungsten masks spot-welded onto a TZM plate, to prevent space charge limitation and to shield the RFEA from heat damage. (d) The RFEA installed in the Sample Exposure Chamber, facing a deuterium ion beam.

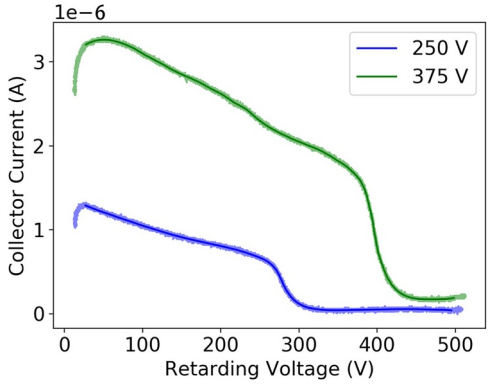

Fig. 4. The RFEA I-V characteristics for nominal output beam energies of 250V and 375V.

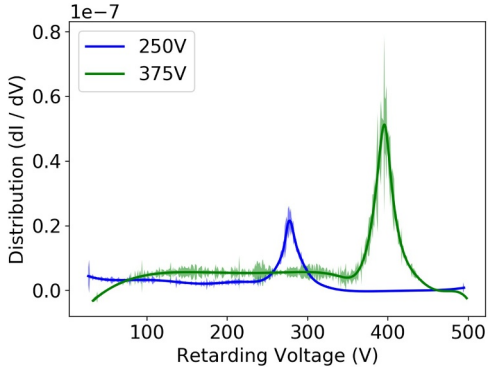

Fig. 5. Differentiated I–V characteristics for nominal output beam energies of 250 V and 375 V, which are related to the ion distribution functions (a.u.). Distinct peaks can be seen near the nominal beam energy.

analyzer and protecting the body from heat damage.

The RFEA was tested in the Sample Exposure Chamber (SEC) in T_i mode. The SEC is a linear device designed to investigate the hydrogen isotope retention properties of lithium, by shining an ion beam directly onto a lithium coated surface. The RFEA is installed such that the axis of the analyzer is aligned with the axis of the ion beam, provided by a gen-2 Tectra plasma source (Fig. 3d). The plasma source, fueled with argon gas, was analyzed at 250 V and 375 V nominal beam energy, which is defined by the source anode voltage. The I–V characteristics are shown in Fig. 4. The ion energy distributions are obtained by differentiating the I–V characteristics, shown in Fig. 5 [16]. The ion distributions show distinct peaks near the nominal output energies, but shifted slightly higher, possibly as a result of the internal plasma potential of the ion source. This demonstrates that the RFEA is working as expected in T_i mode.

Moving forward, the RFEA will be installed onto LTX-β at the LFS midplane with a rotary feedthrough, such that its axis can be aligned with the magnetic field, and rotated to collect both co-moving and counter-moving particles. The ion distribution will be measured with the T_i mode grid potential configuration, at various radial locations. In conjunction with the electron temperature measurements that will be provided by the LFS and HFS Langmuir probes, we will be able to find the plasma potential from the RFEA I–V characteristics and compare it with the theoretical predictions made in Section 2.

4. Summary

In this work we present a numerical calculation of the ambipolar potential in the LTX SOL, and the setup and testing of the new RFEA to be installed onto LTX-β.

Based on observations of low edge collisionality from past LTX experimental campaigns, we argue that the majority of particles in the SOL are mirror trapped. The main loss mechanism is therefore pitch angle scattering from trapped to passing orbits, instead of free streaming as in conventional fluid-like SOLs. The resultant ambipolar potential is numerically calculated, and is significantly lower than that predicted by the conventional Debye sheath model. This implies that the ions incident upon the limiting surfaces will be less energetic than previously expected, reducing the sputtering rate. The potential gradient also covers the entire SOL region, instead of being restricted to a narrow region in front of the limiter. The resultant parallel electric field should help with ejecting the sputtered low energy impurity ions and protecting the core plasma from contamination.

To test these predictions, an RFEA has been developed for ion energy and plasma potential measurements in the LTX-β SOL. A set of tungsten masks have been developed to avoid space charge limitations. The RFEA was tested in T_i mode in the Sample Exposure Chamber and successfully characterized a deuterium ion beam. The I-V characteristics and derived distribution functions agree approximately with expectations.

Acknowledgements

This work was supported by US DOE contracts DE-AC02-09CH11466, DE-AC05-00OR22725, and DE-AC52-07NA27344. The authors would like to acknowledge the magnetic geometry data provided by Christopher Hansen, the technical expertise of Enrique Merino, Tom Kozub, and Gus Smalley, and helpful discussions with Paul Hughes and Nicolas Lopez.

References

[1] L.E. Zakharov, N.N. Gorelenkov, R.B. White, S.I. Krasheninnikov, G.V. Pereverzev, Ignited spherical tokamaks and plasma regimes with LiWalls, Fusion Eng. Des. 72 (1–3) (2004) 149, https://doi.org/10.1016/j.fusengdes.2004.07.015.

[2] S.I. Krasheninnikov, L.E. Zakharov, G.V. Pereverzev, On lithium walls and the performance of magnetic fusion devices, Phys. Plasmas 10 (5) (2003) 1678, https://doi.org/10.1063/1.1558293.

[3] D.P. Boyle, R. Majeski, J.C. Schmitt, C. Hansen, R. Kaita, S. Kubota, M. Lucia, T.D. Rognlien, Observation of flat electron temperature profiles in the lithium tokamak experiment, Phys. Rev. Lett. 119 (1) (2017) 015001, https://doi.org/10.1103/PhysRevLett.119.015001.

[4] R. Majeski, R.E. Bell, D.P. Boyle, R. Kaita, T. Kozub, B.P. LeBlanc, M. Lucia, R. Maingi, E. Merino, Y. Raitses, J.C. Schmitt, J.P. Allain, F. Bedoya, J. Bialek, T.M. Biewer, J.M. Canik, L. Buzi, B.E. Koel, M.I. Patino, A.M. Capece, C. Hansen, T. Jarboe, S. Kubota, W.A. Peebles, K. Tritz, Compatibility of lithium plasma-facing surfaces with high edge temperatures in the lithium tokamak experiment, Phys. Plasmas 24 (5) (2017) 056110, https://doi.org/10.1063/1.4977916.

[5] R. Majeski, R.E. Bell, D.P. Boyle, P.E. Hughes, T. Kozub, R. Lunsford, E. Merino, X. Zhang, T.M. Biewer, J.M. Canik, D.B. Elliott, M. Reinke, M.A. Dorf, T. Rognlien, F. Scotti, V. Soukhanovskii, S. Kubota, T. Rhodes, J.K. Anderson, C. Forest, J. Goetz, S. Oliva, D. Donovan, R. Kaita, A. Maan, T. Jarboe, C. Hansen, L. Buzi, B.E. Koel, L.E. Zakharov, The LTX-β Research Program and First Results, to be published in Nuclear Fusion Special Issue: overview and summary reports from the 27th Fusion Energy Conference, Gandhinagar, India, 2018 22–27 Oct, 2018.

[6] D.E. Baldwin, End-loss processes from mirror machines, Rev. Mod. Phys. 49 (2) (1977) 317, https://doi.org/10.1103/RevModPhys.49.317.

[7] V.P. Pastukhov, Collisional losses of electrons from an adiabatic trap in a plasma with a positive potential, Nucl. Fusion 14 (1) (1974) 3, https://doi.org/10.1088/0029-5515/14/1/001.

[8] D.P. Chernin, M.N. Rosenbluth, Ion losses from end-stoppered mirror trap, Nucl. Fusion 18 (1) (1978) 47, https://doi.org/10.1088/0029-5515/18/1/008.

[9] R.H. Cohen, M.E. Rensink, T.A. Cutler, A.A. Mirin, Collisional loss of electrostatically confined species in a magnetic mirror, Nucl. Fusion 18 (9) (1978) 1229, https://doi.org/10.1088/0029-5515/18/9/005.

[10] J.D. Huba, NRL Plasma Formulary, Naval Research Laboratory, Washington, DC 20375, 2011.

[11] C. Hansen, D.P. Boyle, J.C. Schmitt, R. Majeski, Equilibrium reconstruction with 3d eddy currents in the lithium tokamak experiment, Phys. Plasmas 24 (4) (2017) 042513, https://doi.org/10.1063/1.4981214.

[12] D. Brunner, B. LaBombard, R. Ochoukov, D. Whyte, Scanning retarding field analyzer for plasma profile measurements in the boundary of the Alcator C-mod tokamak, Rev. Sci. Instr. 84 (3) (2013) 033502, https://doi.org/10.1063/1.4793785.

[13] I.H. Hutchinson, Principles of Plasma Diagnostics, 2nd ed., Cambridge, 2002, https://doi.org/10.1017/CBO9780511613630.

[14] T. Honzawa, T. Sekizawa, Y. Miyauchi, T. Nagasawa, Effects of space charges in gridded energy analyzer, Jpn. J. Appl. Phys. 32 (12R) (1993) 5748, https://doi.org/10.1143/JJAP.32.5748.

[15] D. Brunner, B. LaBombard, R. Ochoukov, R. Sullivan, D. Whyte, Space-charge limits of ion sensitive probes, Plasma Phys. Control. Fusion 55 (12) (2013) 125004, https://doi.org/10.1088/0741-3335/55/12/125004.

[16] C. Bohm, J. Perrin, Retarding-field analyzer for measurements of ion energy distributions and secondary electron emission coefficients in low-pressure radio frequency discharges, Rev. Sci. Instr. 64 (1) (1993) 31, https://doi.org/10.1063/1.1144398.